Nanoscale

PAPER

View Article Online
View Journal | View Issue

Cite this: *Nanoscale*, 2023, **15**, 13728

Nanotechnology and narasin: a powerful combination against acne

Fatima Abid,[a] Bhumika Savaliya,[b] Ankit Parikh,[a] Sangseo Kim,[a] Marzieh Amirmostofian,[a] Laura Cesari,[c] Yunmei Song,[a] Stephen W. Page,[d] Darren J. Trott[b] and Sanjay Garg *[a]

Acne vulgaris is widely regarded as the most prevalent skin disorder characterized by painful, inflammatory skin lesions that are primarily attributed to the pathogenic actions of *Cutibacterium acnes* (*C. acnes*). To improve the clinical management of this disease, there is a pressing clinical demand to develop innovative antibacterial therapies that utilize novel mechanisms. The current research aimed to discover the antibacterial efficacy of narasin (NAR), a polyether ionophore, against drug-resistant acne bacteria. In addition, the study aimed to formulate self-nanomicellizing solid dispersions (SNMSD), utilizing Soluplus® (SOL), as a drug delivery system to incorporate NAR and selectively target the lipophilic *C. acnes* abundant environments within the skin. Furthermore, the study aimed to investigate the *ex vivo* deposition and permeation of NAR into the various layers of the skin using full-thickness porcine ear skin as a model skin. By encapsulating NAR within spherical polymeric micelles (d_n < 80 nm) aqueous solubility was significantly increased by approximately 100-fold (from <40 μg mL^{-1} to 4600 μg mL^{-1}). Following optimization, the micelle solution was integrated into a gel formulation (containing 0.2% w/v NAR) and evaluated for stability over 4 weeks at room temperature (drug content >98%). Results from drug deposition and permeation experiments demonstrated that the deposition of NAR from the NAR-micelle solution and its gel formulation into the lipophilic stratum corneum (19 835.60 ± 6237.89 ng cm^{-2} and 40 601.14 ± 3736.09 ng cm^{-2}) and epidermis (19 347 ± 1912.98 ng cm^{-2} and 18 763.54 ± 580.77 ng cm^{-2}) was superior to that of NAR in solution, which failed to penetrate any skin layers. In conclusion, the outcomes of this study provide evidence that NAR exhibits promising activity against antimicrobial resistant strains of *C. acnes* (MIC range ≤0.008–0.062) and that micelle nanocarriers can improve the aqueous solubility of poorly water-soluble drugs. Furthermore, our results highlight the ability of nanomicelles to enable selective and targeted drug delivery to the lipophilic skin layers.

Received 18th April 2023,
Accepted 4th August 2023

DOI: 10.1039/d3nr01789c

rsc.li/nanoscale

1 Introduction

Acne vulgaris is the eighth most prevalent inflammatory skin disease of humans worldwide associated with bacteria-induced skin lesions.[1,2] It severely impacts 9.4% of the global population with adolescents aged between 14 to 19 years affected more than adults.[1,3,4] Indeed, acne is not a physically serious ailment, however, its psychosocial impacts are well documented.[2,4] At the crucial developmental stage of adolescence, acne is associated with a significant decline in the psychological and emotional well-being of individuals.[4] Social embarrassment from residual facial scarring and related psychological disturbances such as depression, anxiety, social isolation, poor self-image, and low self-confidence leads to significant morbidity and poor quality of life.[4,5]

The leading attributions among individuals diagnosed with acne disorder are genetics,[6] diet,[7] age, hormonal disturbance,[8] hyperplasia of the sebaceous gland, excessive production of sebum, pilosebaceous unit obstruction due to altered growth of follicles and comedones, localized inflammation and colonization of pilosebaceous glands by *Cutibacterium acnes* (*C. acnes*), previously known as *Propionibacterium acnes*.[9] Even though acne has multifactorial aetiologies, the pilosebaceous colonization by *C. acnes*, *Staphylococcus aureus* (*S. aureus*), and *Staphylococcus epidermidis* (*S. epidermidis*) makes the most significant contribution to its pathogenesis causing the development of inflammatory lesions.[10] Due to multiple aetiologies, the pathogenesis of acne is therefore complex and still evolving.[11]

[a]*Clinical and Health Sciences, University of South Australia, Adelaide, SA 5000, Australia. E-mail: Sanjay.garg@unisa.edu.au*
[b]*Australian Centre for Antimicrobial Resistance Ecology, School of Animal and Veterinary Sciences, University of Adelaide, Roseworthy SA, 5371, Australia*
[c]*Faculty of Pharmacy, Aix-Marseille Université, Marseille 13007, France*
[d]*Luoda Pharma, Newtown, NSW 2042, Australia*

Even though there are many options for acne treatment, the profile of detrimental, long-lasting side effects remains significantly poor. With bacteria having a critical role in the pathogenesis of acne, oral antibiotics are the most used agents for acne therapy.[12] However, the long-term use of antibiotics has inevitably led to the development of antibiotic resistance, presenting a major problem for the effective treatment of infectious dermatologic diseases.[12,13] Topical antibiotic formulations are associated with high levels of antibiotic resistance by *C. acnes* and systemic antibiotics impose serious systemic side effects.[14] Therefore, to minimize exposure to systemic adverse effects and the emergence of resistance there is a need to develop a new antibacterial therapy that is both effective and safe for acne therapy.

Carboxylic polyether ionophores are compounds that are marketed as anticoccidial drugs globally for poultry and ruminants (such as cattle, sheep, and goats). At approved feed levels, these compounds are effective and safe. They form reversible dynamic complexes with cations that are soluble in lipids and by this means enable the transport of specific ions across biological membranes. Through this mechanism, polyether ionophores have antibacterial activity as well.[15]

Narasin (NAR), produced by *Streptomyces aureofaciens*, is a newer polyether antibiotic.[16] It is known to exhibit antibacterial, antiprotozoal, antifungal, and antiviral[17] properties. One previous study has confirmed its effectiveness against Gram-positive bacteria, however, its role in acne treatment caused by *C. acnes* has never been investigated. NAR is structurally similar to salinomycin, being the 3-methyl-analogue, and is similarly insoluble in water[16] with log *P* o/w of 6.20, meaning it is highly lipophilic and therefore its formulation is a challenging task.

The topical delivery system for antiacne drugs is a preferred choice by patients and clinicians to reduce the risk of unwanted adverse effects of systemic administration.[18] The skin, however, provides a barrier to penetration of the hair follicle sites of infection by topically administered highly lipophilic and hydrophilic drugs.[18] For this reason, much of the current literature on optimizing the dermal delivery of drugs pays attention to nanocarriers as novel topical delivery systems as they allow enhanced cutaneous permeation to hair follicle sites.[19] The polymeric micelles, among recent nanoparticle-mediated hair follicle-targeted delivery investigations, have demonstrated significant potential to enhance hair follicle permeation and increase drug loading efficiency, thereby minimising the dose-related adverse effects of formulations.[20–26] To achieve an optimal NAR therapeutic effect, targeted delivery to the follicular epithelium is essential. This can be achieved by developing an aqueous polymeric nano-micelle that may enable increased cutaneous permeability and partitioning of NAR into the lipophilic epidermis.

Nano-micelle formulations were prepared using Soluplus® (SOL), a novel non-ionic bifunctional fourth-generation amphiphilic copolymer that actively solubilizes poorly aqueous soluble drugs by maintaining supersaturation at the target site. SOL has a hydrophilic–lipophilic balance (HLB) value of 14 and possesses a very low critical-micelle concentration of 7.6 mg mL^{-1}, rendering it an ideal candidate for the design of targeted drug delivery systems.[27] SOL has been used previously to improve the therapeutic effectiveness and aqueous solubilities of various drugs including curcumin,[28] danazol,[29] itraconazole,[29] fenofibrate,[29] quercetin,[30] fenbendazole,[31] carvedilol,[32] and aprepitant.[33] Furthermore, its use in topical formulations[34,35] has also been reported including acne treatment using nicotinamide.[36]

To the best of our knowledge, no nanoformulation including polymeric nano-micelle formulation for NAR has previously been developed. The specific purpose of the present research was: (1) to discover, for the first time, new antibacterial properties of NAR against resistant acne infections, (2) to improve the aqueous solubility of NAR by developing novel NAR-loaded self-nano-mineralising solid dispersion systems (SNMSD), (3) to develop and optimise a micelle-gel formulation for targeted delivery to cutaneous site, and lastly (4) to investigate *ex vivo* distribution and permeation of NAR from the micelle-core into the stratum corneum, epidermis and dermal skin layers.

2 Experimental

2.1 Materials and methods

NAR, Monensin (MON), and SOL were a generous gift from Luoda Pharma (Newtown, NSW, Australia) and BASF Australia Ltd (Victoria, Australia), respectively. Hydroxypropyl methylcellulose-ASMG (HPMC-ASMG) and hydroxypropyl methylcellulose-ASLG (HPMC-ASLG) were obtained from Mayne Pharma International (South Australia, Australia). Sodium hydroxide pellets, phosphoric acid, and acetic acid were obtained from Chem Supply (South Australia, Australia). Concentrated hydrochloric acid (HCL), disodium hydrogen phosphate, formic acid, and citric acid were obtained from Sigma-Aldrich (New South Wales, Australia). Boric acid was obtained from Optigen Scientific (South Australia, Australia). Throughout the study, ultra-pure water sourced from a Millipore ultra-pure water system was utilized, whereas all other chemicals were of analytical grade. Dimethyl sulfoxide (DMSO) and HPLC-grade methanol were ordered from Merck (Melbourne, VIC, Australia). Hydroxyethyl cellulose (HEC) was ordered from Medisca (New York, USA), sodium carboxymethyl cellulose (NaCMC) from Aldrich Chemistry (Missouri, USA), hydroxypropyl methylcellulose (HPMC) from Triway Chemical Ltd (Guangzhou, China), and Carbopol® 974 P was obtained from Lubrizol pharmaceuticals (Victoria, Australia). 3-(4,5-Dimethylthiazol-2-yl)-2,5-diphenyltetrazolium bromide (MTT) was obtained from Life Technologies Australia (Mulgrave, Australia). Dulbecco's modified Eagle's medium (DMEM) high glucose, Gibco™ HEPES (*N*-2-hydroxyethyl piperazine-*N*-2-ethane sulfonic acid, Gibco™ MEM non-essential amino acids (NEAA), and fetal bovine serum (FBS) were ordered from ThermoFisher Scientific (Victoria, Australia), penicillin/streptomycin, Dulbecco's phosphate buffered saline (PBS),

L-glutamine were ordered from Sigma-Aldrich (New South Wales, Australia). HEPES, and NEAA. Brucella agar base and Sheep blood were ordered from ThermoFisher Scientific (Victoria, Australia) and hemin, vitamin K1 and clindamycin were ordered from Sigma-Aldrich (New South Wales, Australia).

2.2 Analytical method

2.2.1 Quantification of NAR by HPLC method. The HPLC method using a refractive index (RI) detector was utilized as previously reported.[37] A Phenomenex C18 (4.6 × 150 mm, 5 μm) analytical column was used with the mobile phase composed of methanol (92 mL), glacial acetic acid (1 mL), and Milli Q water (8 mL). The column oven temperature, flow rate, and injection volume used were 30 °C, 1 mL min^{-1}, and 50 μL, respectively.

2.2.2 Quantification analysis of NAR by LC-MS/MS. The quantities of NAR that were deposited in the skin, as well as those that penetrated across the skin during the *in vitro* deposition assay, were quantified using LC-MS/MS analysis. The Shimadzu 8030 TripleQuad LC-MS/MS (Shimadzu, Kyoto, Japan) was used in positive mode with electrospray ionization (ESI) to analyse the samples. A 5 μL injection volume of each sample (blank, zero, standards, QCs and unknown) was loaded onto a Phenomenex Kinetex C18 analytical column, 100 Å (50 × 3 mm, 2.6 μm), with a flow rate of 0.3 mL min^{-1}. The column and syringe temperatures were 40 °C and 15 °C, respectively. The mobile phases used for LC separation were milliQ water containing 0.1% formic acid (A) and methanol containing 0.1% formic acid (B). The gradient elution was summarized as follows: 0.1–2.0 min, 10% B; 2.0–10.0 min, 10% to 90% B; 10.0–20.0 min, 90% B; and 20.0–22.0 min, 10% B. The total analysis required 22 min.

The evaluation was executed using an MRM (multiple reaction monitoring) technique, developed through optimization of precursor ion and product ion transitions. Within the scope of NAR and MON, two primary precursor ion/product ion transitions with high intensity were detected. The quantifier ion was determined based on the response obtained from both transitions, with the ion exhibiting the highest response selected as the quantifier, and the other as the qualifier ion. The MRM transitions for NAR were 787.0 to 431.0 (CE: −60) and 787.0 to 531 (CE: −35) with a dwell time of 100. The MRM transitions for MON were 693.0 to 675.3 (CE: −50) and 693.0 to 479.3 (CE: −50) with a dwell time of 100. Also, the nebulizing gas flow and the dry gas flow were 2 and 15 L min^{-1}, respectively. DL temperature was 250 °C and heat block temperature was 400 °C.

2.2.3 Calibration points and sample preparation. For LC-MS/MS analysis, 10 different concentrations of NAR were prepared as calibration standards (from 10 to 2000 ng mL^{-1}) by dilution of the stock solution of 1 mg mL^{-1} of NAR in methanol. A blank was methanol and a zero-point contained only IS, which was MON (400 μg mL^{-1} in methanol). Three different concentrations were prepared of quality control (QC) samples as low, medium, and high QC. All sample (blank, zero, standards, QCs and unknown) were prepared for LC-MS/MS analysis by mixing 50 μL of samples with 10 μL IS.

2.2.4 Validation of analytical method. The validation study incorporated several parameters, including selectivity, sensitivity, linearity, precision, and accuracy, with inter-day and intra-day repeatability being considered for accuracy evaluation.

To evaluate the selectivity, the MS chromatograms of a blank sample was compared with a spiked blank sample containing ten different levels of NAR concentration along with the IS (MON), which were analysed in four replicates. The linear calibration curves were created by correlating the ratio of NAR peak area to IS peak area (*y*-axis) to NAR standard concentration (*x*-axis). The developed LC-MS/MS method was found to be linear in the concentration range between 10–2000 ng mL^{-1} with a regression coefficient (R^2) of 0.998. The sensitivity assessment procedure entailed the measurement of the NAR response in several diluted solutions derived from a concentrated working solution. This process continued until the signal-to-noise ratio (S/N) approached a value of approximately 3, which was deemed the limit of detection (LOD) and a value of 10 for the limit of quantification (LOQ). The LOD for NAR was estimated to be approximately 3 ng mL^{-1}, and the LOQ was found to be 10 ng mL^{-1}. The intra- and inter-day accuracy and precision were determined by replicate analysis of three different concentrations. The intra-day/inter-day precision was determined as the relative standard deviation (RSD) and found to be 0.06/0.72, 0.46/0.32, and 0.14/0.66 for low, medium, and high concentration, respectively. The accuracy was defined as mean of recoveries (%) ± RSD and found to be 101.19 ± 0.46, 100.84 ± 0.47, and 102.98 ± 0.15 respectively for the same concentrations.

2.3 Formulation development and optimization

2.3.1 Preparation of NAR self-nano-micellizing solid dispersion. Three polymers were selected namely SOL, HPMC-ASLG and HPMC-ASMG to prepare three SNMSDs using the solvent evaporation method with the drug/polymer ratio 1 : 5. To prepare SOL-based SNMSD (F1), NAR and SOL were dissolved in dichloromethane whereas HPMC-based SDs (F2 using HPMC-ASMG, and F3 using HPMC-ASLG) were developed by dissolving NAR in a mixture of dichloromethane and acetone. Each solution was evaporated using a rotary evaporator under a vacuum (Büchi Rotavapor® R-210, Switzerland) at a controlled temperature. The temperature was kept between 32 °C–36 °C for F1 and 34 °C–50 °C for F2 and F3. The dried SNMSDs were scraped from the flask into mortar-pestle using a spatula, pulverised, and sieved through a 250 μm sieve to obtain a uniform powder. Each SNMSD sample was kept in a desiccator overnight for drying and stored at room temperature for further studies including characterisation studies.

2.3.2 Determination of NAR solubility in micelle formulations. The improvement in the aqueous solubility of NAR in micelle formulations was determined in phosphate buffer solution (PBS) pH 7.40. Briefly, an excess amount of NAR (50 mg) or equivalent dispersion (300mg) was transferred in

10 mL PBS at ambient temperature. The samples were continuously rotated using a multitube vortex (RATEK Instruments MTV1, Australia) for 5 hours and then transferred to an orbital mixer incubator (RATEK, Australia) for overnight mixing. Solubility samples (2 mL) were collected after 24 h, filtered through a 0.45 μm PVDF syringe filter, and transferred to HPLC vials for solubility analysis.

2.4 Characterization of micelle formulation

2.4.1 Determination of NAR in micelle. Total NAR content was quantified by the HPLC method. The NAR entrapped in the micelles was determined by dissolving 6 mg of F1-micelle in 2 mL of methanol and vortexed the mixture for 5 min. The following equations[26] were used to calculate NAR content, drug loading, and incorporation efficiencies:

$$\text{Drug content(mg drug per mL formulation)} = \frac{\text{mass of NAR in the formulation(mg)}}{\text{the volume of the formulation(mL)}}$$

$$\text{Drug loading(mg drug per g copolymer)} = \frac{\text{NAR in the formulation(mg mL}^{-1}\text{)}}{\text{the copolymer in the formulation(g mL}^{-1}\text{)}}$$

$$\text{Incorporation efficiency(\%)} = \frac{\text{mass of NAR incorporated into micelles(mg)} \times 100}{\text{mass of NAR introduced(mg)}}$$

2.4.2 Size characterization. Micelle formulation was characterised using Malvern Zetasizer Nano-ZS (Worcestershire, UK) by its particle size, and polydispersity index (PDI). The formulations were diluted in 1 : 100 using MilliQ water and measurements were taken in triplicates at a 25 °C temperature.

2.4.3 Morphology. Surface morphology for the samples including NAR, SOL, and NAR-micelle was studied with a Zeiss Merlin field emission gun scanning electron microscope (SEM) (Jena, Thuringia, Germany). Before analysis, the samples were mounted on SEM stubs using conductive double-sided adhesive tape, subjected to sputter coating with platinum (approximately 5 nm) and then examined at the magnification of 100× using a 2.00 kV accelerating voltage.

The transmission electron microscopy (TEM) using a Techani G2 Spirit TEM, (FEI Company, Hillsboro, OR, USA) operating at 100 kV was used to further analyse the micelle morphology. Briefly, 5 μL of the sample was spotted and left to adhere for 2 min on cleaned formvar/carbon-coated thin 200 mesh copper grids glow discharged for 15 s using GATAN Solarus 950 Advanced Plasma Cleaner. Excess liquid was removed using filter paper and a drop of water was added. Consequently, the grid was put in contact with 5 μL of 2% uranyl acetate aqueous solution for 2 min and allowed to air-dry before recording TEM images.

2.4.4 Differential scanning calorimetry (DSC). The NAR, SOL, and F1-micelle samples were subjected to DSC analysis using a Discovery DSC TA Instruments (Model 2920, New Castle, DE, USA) to determine their thermal properties. Dry samples (2–4 mg) were analysed in an aluminium crucible by heating at a rate of 10 °C min^{-1} (25 °C to 250 °C) under a nitrogen atmosphere (50 mL min^{-1}).

2.4.5 Fourier transform infrared (FTIR) spectroscopy. FTIR spectra of NAR, SOL, NAR-SOL physical mixture, and F1 micelle were obtained using the FTIR instrument (ATR-FTIR Perkin Emler spectrum 400 USA). At the frequency range of 4000–400 cm^{-1} and a resolution of 4 cm^{-1} with 16 scanning rates, the spectra were recorded. Small quantities of each powder were placed on the ATR diamond crystal on the instrument and the samples were secured in contact with the diamond crystal by exerting force with the clamp. The background correction was performed before each reading.

2.5 Assessment of self-nanomicellizing properties of NAR-micelle

2.5.1 Preparation of micelle-gel formulations. The optimized NAR micelle formulation was developed into a gel as a suitable dosage form for topical applications. Different polymers namely HEC, Na-CMC, HPMC, and Carbopol 974 P were initially screened during the formulation development. HEC was, however, selected and further tested using different concentrations (1%, 1.5%, and 2%). The optimised gel was prepared by incorporating polymer in appropriate amounts to the micelle solution (0.2%) maintained at 25 °C temperature using a magnetic hot plate and speed set at 250 rpm for 4 h.

2.5.2 Characterization of micelle-gel formulations. The developed micelle-gel formulation (F1-gel) was characterized in triplicates for its pH using a pH meter (PerpHecT® ROSS® Micro electrode; Thermo Scientific; Massachusetts, USA) and rheological properties using a Rheometer a Rheosys Merlin VR (Scientex Pty Ltd, Melbourne, Victoria, Australia) using a parallel plate with a diameter of 15 mm. The content of NAR in micelle formulation was also determined as mentioned above (section 2.4.1).

2.5.3 Stability study. The stability of the micelle formulation was investigated after storage at 25 °C/60% RH for 4 weeks in tightly closed glass bottles (days 1, 14, and 28). The NAR content was determined by the HPLC method after collecting samples at predetermined time intervals.

2.6 *In vitro* minimal inhibitory concentrations (MIC) testing

2.6.1 Bacterial strains and growth conditions. For this study thirty-one *Cutibacterium acnes* (*C. acnes*) clinical isolates were sourced from Dr J. Robson (Sullivan Nicolaides Pathology, Bowen Hills, Queensland) and were subcultured on Brucella agar plates that were supplemented with 5% v/v laked sheep blood, vitamin K1, and hemin. Plates were then incubated anaerobically at 37 °C for 48 hours. Isolate identification was confirmed by MALDI-TOF and isolates were stored in glycerol broth at −80 °C until used. *Bacteroides fragilis* (*B. fragilis*) ATCC (American Type Culture Collection) 25285 was used as a quality control strain and was tested against clindamycin. Apart from these clinical isolates *Staphylococcus aureus* (*S. aureus*) ATCC 29213 and *Staphylococcus epidermidis* (*S. epidermidis*) ATCC 14990 were also tested in this study.

2.6.2 MIC testing. MICs of anaerobic *C. acnes* and *B. fragilis* were determined by the Agar dilution method. As Per CLSI guidelines,[38] Brucella agar medium, fortified with hemin (5 μg mL^{-1}) and vitamin K1 (1 μg mL^{-1}), was formulated and subjected to autoclaving. The stock solutions of NAR, F1, F2, and F3 were prepared at least 10 times the highest antibacterial agent concentration to be tested and then two-fold serial dilutions were made depending on the testing concentration range. NAR stock solution was prepared using methanol whilst PBS was used to solubilise F1, F2, and F3. To prepare agar dilution plates containing agar (20 mL) laked sheep blood (1 mL) and 10× antimicrobial agent solution (2 mL) were added to molten brucella agar (17 mL) supplemented with hemin and vitamin K1. Plates were allowed to solidify and then were inoculated by the isolates. Isolates were subcultured twice on the agar plates and direct colony suspension was used to obtain bacterial inoculum equivalent to a 0.5 McFarland standard as determined by the nephelometer. To apply 1–2 μl inoculum on an agar surface inoculum-replicating apparatus was used. The final inoculum will then be about 10^5 CFU per spot on the agar. The final tested concentration ranges of the formulations for *C. acnes*, *S. aureus* ATCC 29213 and *S. epidermidis* ATCC 14990 were 0.008–0.062 μg mL^{-1}, 0.125–4 μg mL^{-1} and 0.125–4 μg mL^{-1}, respectively while *B. fragilis* ATCC 25285 was tested against the range of 0.25–4 μg mL^{-1} clindamycin. Additionally, a negative growth control plate without any bacterial inoculum and a positive growth control plate with inocula but without antibacterial agents were also prepared. Plates with anaerobes were then incubated anaerobically at 37 °C for 48 hours and staphylococcal isolates plates were incubated aerobically at 37 °C for 24 hours.

2.6.3 Determination of MICs. After incubation, agar plates were assessed visually to determine any growth. The antimicrobial MIC values were documented as the lowest concentration at which bacterial growth was inhibited. Test system performance was monitored based on MIC results obtained for the ATCC control strain (*B. fragilis* ATCC 25285) against the control antimicrobial clindamycin. The control antimicrobial QC range is outlined below in Table 3. Negative growth control plates must remain clear. Positive growth control plates were required to exhibit an acceptable level of growth for tests to be considered valid.

2.7 *In vitro* cytotoxicity assay

The effect of formulations on human foreskin fibroblast (HFF-1) and keratinocyte (HaCaT) cell viability was evaluated by MTT assay. HFF and HaCat cells were cultured separately in T75 sterile culture flasks with high glucose DMEM. The cells were supplemented with FBS (15% for HFF-1; 10% for HaCaT), 1% pen–strep, 1% L-glutamine, 1.5% HEPES, and 1% NEAA under 5% CO_2 at 37 °C in a humidified incubator. The media was changed every 48 h to reach 90% confluency. Thereafter, the cells were seeded on 96-well plates with 100 μL culture media for 24 h incubation. The following day, the samples (75 μL) were added, and incubated for another 24 h. A series of serial dilutions were tested between concentrations 0.01 to 4 μg mL^{-1}. The negative controls were also set up including the untreated cells. The following day, the cells were gently rinsed twice with PBS and incubated for 4 h with 10 μL of MTT solution. DMSO was then added after removing the MTT solution from each well to dissolve the MTT formazan crystals. Using the microplate plate reader by PerkinElmer Wallac (PerkinElmer, Inc., Waltham, MA, USA) the absorbance was recorded at 570 nm. The results were determined as percentage viability.

2.8 Evaluation of *in vitro* NAR delivery

2.8.1 Skin preparation. Full-thickness pig ear skin samples collected from a local slaughterhouse were used for the study.[39] Briefly, the skin samples were cleaned with MilliQ water, and the hair was trimmed carefully using a hair clipper. The skin was separated from the ear cartilage and then stored at −20 °C until further use. The skin was cut into 1 mm thick circular disks (25 mm diameter) for each permeation experiment.

2.8.2 *Ex vivo* permeation and deposition studies. At the start of each study, skin samples were thawed to room temperature and integrity was determined by recording the transepithelial electrical resistance (TEER) using an MM400 digital multimeter (Klein Tools, Australia).[40] The skin samples were then fixed in Franz diffusion cells facing the stratum corneum side upwards. 5 mL of phosphate buffered solution (pH 7.4) was added in the receiver chamber and 1 g finite dose of formulation (F1-micelle and F1-gel) and control (NAR-water) was applied in the donor chamber corresponding to 2 mg cm^{-2} and 0.04 mg cm^{-2} of NAR respectively, after reaching equilibrium. The receptor compartment was consistently maintained at a temperature of 34 °C and continuously agitated throughout the experiment using a magnetic stirrer. At regular time intervals (1 h, 2 h, 4 h, 8 h, 12 h, and 24 h), aliquots of 200 μL were collected and analysed by the developed LCMS method to determine the amount of NAR permeated across the skin. To maintain sink conditions, the amount of aliquot collected was replaced with an equal amount of fresh PBS. The samples were collected and analysed in triplicates.

Following 24 hours, the Franz diffusion cells were disassembled, and the surface of the skin was delicately cleansed with a cotton-tipped applicator to remove any remaining formulation. The skin surface exposed to the formulation was then rinsed using 10 mL MilliQ water and allowed to dry at room temperature before performing the deposition study. Subsequently, the skin was mounted on a flat surface using tape, exposing the formulation's contact side upwards. Using the previously reported tape-stripping method,[41] the stratum corneum was removed by using the sampling discs (D100 D-Squame®) 15 times. Firm pressure was applied using the pressure instrument (D500 D-Squame®) and discs were removed using forceps. Afterwards, the epidermis was separated from the remaining skin using forceps and the rest of the skin was dissected into small pieces. Any NAR that penetrated different skin layers was obtained using 10 mL methanol as an

extraction media. The skin samples were soaked overnight for 24 h and continuously stirred to ensure complete extraction of NAR. The extracts were centrifuged at 3500 rpm for 20 min using a centrifuge (Beckman Coulter Allegra X-12R, USA), filtered using a 0.45 μm PTFE syringe filter, diluted (if required) and analysed using LC-MS/MS.

2.9 Data analysis

All experimental procedures were conducted in triplicate and the outcomes were presented as mean values accompanied by standard deviations (SD) unless otherwise specified. The statistical significance of the distinctions between the treated and control samples was evaluated through the employment of the ANOVA test. Statistical significance was considered as $p < 0.05$, as revealed by the GraphPad Prism software (version 9.4.1, CA, USA).

3 Results and discussion

3.1 Development of an optimized micelle formulation

The poor aqueous solubility and high lipophilicity of drugs pose a serious pharmaceutical hurdle to the development of an effective formulation. The development of micelles made from copolymers has emerged as an effective approach for solubilizing such drugs, ultimately improving their therapeutic efficacy. To explore the effect of polymers on NAR incorporation and solubility improvement, a series of NAR-micelles were developed using short-listed polymeric carriers. As the incorporation of NAR in the drug carrier depends on its miscibility and potential affinity with the polymer, therefore, three polymers namely SOL, HPMC-ASLG, and HPMC-ASMG were selected to prepare F1, F2, and F3 micelles respectively to determine the effect on NAR incorporation.

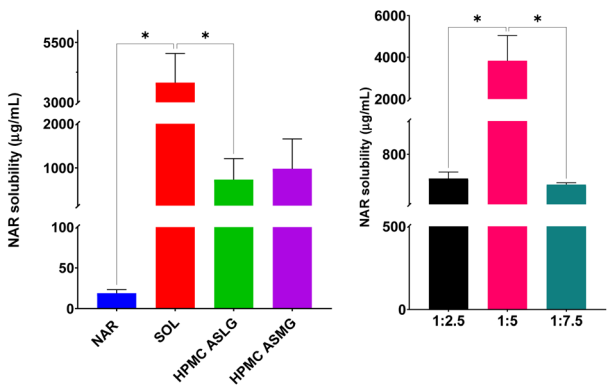

Fig. 1 (A) NAR solubility in SOL, HPMC-ASLG, HPMC-ASMG, (B) effect of SOL concentration on NAR quantity in the micelles. Ordinary one-way ANOVA with Tukey's multiple comparisons. *, $p < 0.05$, mean ± SD.

It was found that NAR incorporation was significantly improved from 42.89 μg mL^{-1} to 4683 μg mL^{-1} (approximately 100 folds) using SOL as a polymeric carrier in F1, and an increase to 1070 μg mL^{-1} (25 folds) for F2 and 1458 μg mL^{-1} (34 folds) for F3 (Fig. 1A). The loading ability and entrapment efficiency of developed micelles were also calculated (Table 1). F1 displayed the highest loading efficiency, indicating minimal loss of NAR during the development process, and therefore was selected for further optimization and characterization. The HPLC analysis was performed using the previously reported method[42] that can detect any degradation peak, which confirms NAR stability during the preparation process. The process losses are a possibility to explain the obtained incorporation efficiencies. There are studies[26,43–48] reported elsewhere suggesting entrapment efficiencies between 75–90%, which coincide with our obtained results. The transition to complete amorphization from crystalline NAR and encapsulation in the polymeric carriers could play a significant role in the formulation of NAR-loaded micelles. The enhancement of the aqueous solubility of lipophilic drugs by SOL due to hydrophobic interaction by hydrogen bonding as reported previously,[49–51] correlates to NAR-enhanced solubility.

The significant improvement in the solubility of a drug also depends on the degree of amorphization and the supersaturated state achieved from the optimal drug-to-polymer ratio. The effect of optimum carrier content could improve the saturation solubility of the undissolved drug by reducing its particle size.[50] It was noted that with the increase in the drug-to-carrier ratio, the saturated solubility of NAR was also increased, highlighting the significance of polymer content on the developed micelles. The NAR displayed the highest solubility in a 1 : 5 ratio of NAR : SOL (1085 μg mL^{-1}) in PBS (pH 7.40) compared to 1 : 2.5 (681 μg mL^{-1}) (Fig. 1B). Based on the results, solid dispersion of NAR : SOL (1 : 5) was finalized for formulation development and further analysis. The higher SOL concentrations were not considered in this study due to the formation of colloidal SOL micelles with increased viscosity, and turbid solutions.[28,52]

3.2 Size and morphology characterization

Particle size is a critical parameter for targeted infundibular delivery. Smaller particle size (600 nm and below) shows efficient penetration to hair follicles, provides greater surface area interface to the target tissue, and hence facilitates delivery of the drug entrapped in the micelle.[53–56] To ensure delivery of

Table 1 Drug content of NAR-micelles

Formulation	Co-polymer content (mg mL^{-1})	Drug loading ± SD (mg g^{-1})	Drug content ± SD (mg mL^{-1})	Incorporation efficiency ± SD (%)
F1	2.5	171.44 ± 3.75	0.441 ± 0.03	85.72 ± 1.88
F2	2.5	168.53 ± 1.67	0.410 ± 0.04	84.26 ± 0.84
F3	2.5	153.37 ± 6.49	0.402 ± 0.04	76.68 ± 3.24

NAR to the targeted site, the particle size of F1-micelles was therefore investigated. The number weighted diameter (d_n) and PDI of NAR micelle was 71.59 ± 0.023 nm and 0.07 ± 0.004, respectively. The size distribution by the intensity of NAR micelles is shown in Fig. 2A. These results coincide with the TEM micrograph of the NAR micelles showcasing the spherical shapes with diameters below 80 nm (Fig. 2B).

3.3 Determination of interaction between SOL and NAR in micelle

Successful development of NAR-micelle depends on the amorphization, micellizing properties and degree of hydrophobic interaction between the NAR and SOL. To determine changes in the solid-state characteristics of NAR in the micelle, differential scanning calorimetry was performed, coupled with scanning electron microscopy to confirm the conversion of NAR from crystalline state to amorphous. FTIR was also conducted to understand the interaction of hydrogen bonds between NAR and SOL.

The melting profile of crystalline NAR, SOL, physical mixture of NAR and SOL, and F1-micelle was determined with DSC and compared to study the solid-state changes. The crystalline NAR exhibited a prominent endothermic peak around 196 °C whereas a thermal peak appeared at 74 °C for SOL displaying its glass transition temperature. However, the physical mixture of NAR and SOL displayed a low intense peak around 190 °C

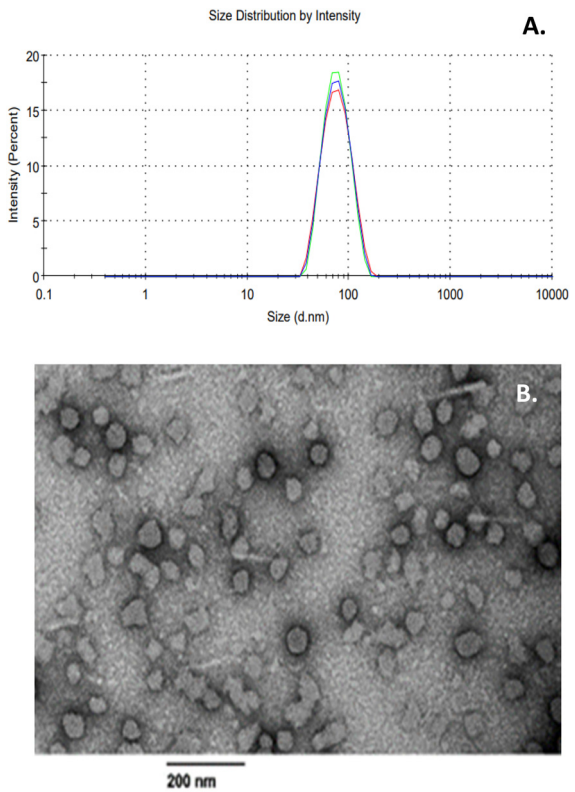

Fig. 2 Size characterisation of NAR micelle formulation: (A) mean particle size (nm) using DLS and (B) TEM image (bar = 200 nm).

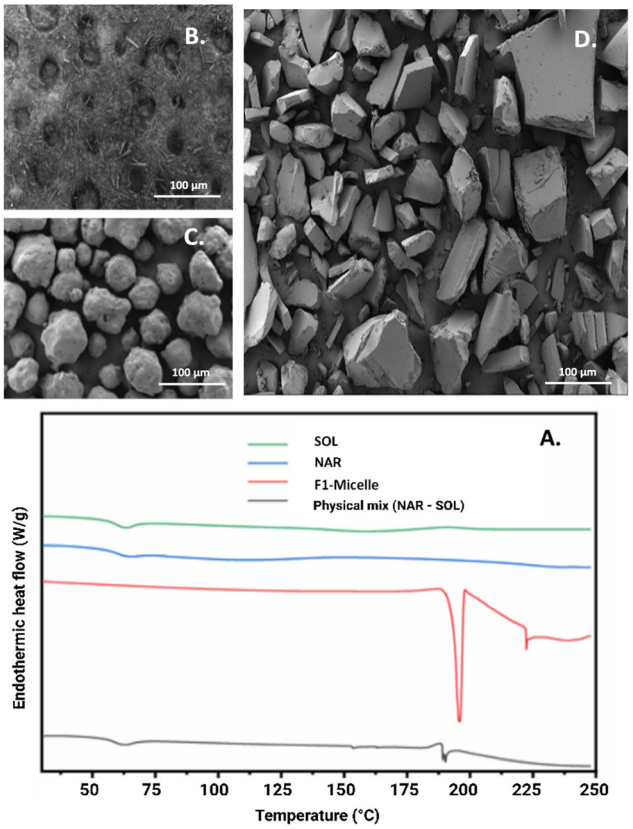

Fig. 3 Characterisation of NAR micelle formulation: (A) DSC thermographs of SOL, NAR, physical mix, and F1-micelle. SEM photomicrograph (bar = 100 µm) of (B) NAR, (C) SOL, and (D) F1-micelle formulation.

(Fig. 3A) whilst no peak appeared for the NAR micelle formulation which validates the complete solid-state transformation in the micelle formulation.

To investigate the surface morphologies of NAR, SOL, and F1-micelle, SEM analysis was used. The crystalline NAR had characteristic needle-shaped structures as shown in Fig. 3B. Fig. 3C displays the micrograph of the irregularly shaped SOL. The SEM micrograph of the irregularly shaped NAR micelles formulation (Fig. 3D) provides observable evidence that the crystalline NAR was fully encapsulated in the micelle and is in strong concurrence with the analysis of DSC. The effect of hydrophobic interaction between SOL and NAR was also investigated using FTIR to comprehend the potential for hydrogen bonding interactions and hence a possible mechanism for the solubilization of NAR in aqueous media. Characteristic signals for NAR were observed at 3388, 2902, 1705, 1455 and 1038 cm^{-1} representing the presence of hydroxyl (–OH), alkane (C–H), aromatic (C═C), aliphatic stretching (C–H), and alkyl amine functional groups respectively (Fig. 4). The peaks typical to SOL appeared at 3469, 2860, and 1732 cm^{-1} showcasing hydroxyl (–OH), aliphatic stretching (C–H), and carbonyl (C═O) groups whereas the IR spectra of physical mix displayed characteristic peaks of both SOL and NAR as shown in Fig. 4, indicating the absence of interaction. Inspecting the F1-

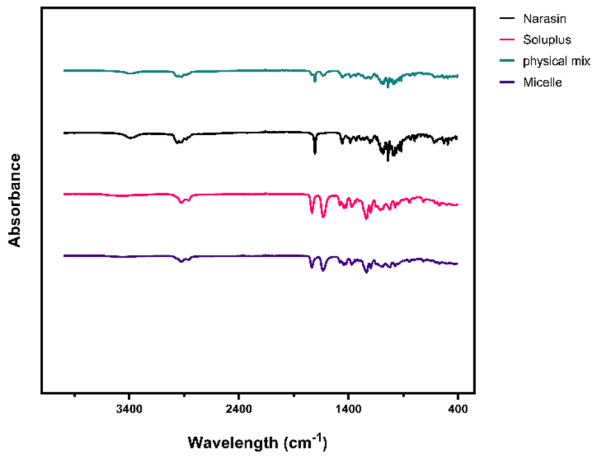

Fig. 4 FTIR spectra of NAR, SOL, NAR-SOL physical mix, and F1-micelle.

micelle IR spectra, however, did not show the typical peak for NAR at 3388 and 1705 cm^{-1} explaining the possibility of full entrapment of NAR in the micelle.

3.4 NAR-micelle gel development and characterization

Blank gels of HEC were prepared at various concentrations between 1.0% to 2.0% w/v and the rheological characteristics were assessed which revealed that the 1% w/v gel had inadequate viscosity compared to 1.5% w/v and 2% w/v concentrations that exhibited satisfactory viscosity and demonstrated shear thinning behaviour (Fig. 5). To enhance the release of micelles containing NAR from the gel matrix, a micelle-gel (F1-gel) was formulated by dispersing 2% HEC in micelle-solution (0.2%). The F1-gel displayed desirable rheological characteristics, as evidenced by Fig. 5, with increasing shear rate, the viscosity of both the blank gel and the F1-gel decreased, with no significant variation observed between them. The content of NAR in F1-gel was 0.2% w/v and its pH of 6.45 ± 0.080 was appropriate for topical application to the skin.[57]

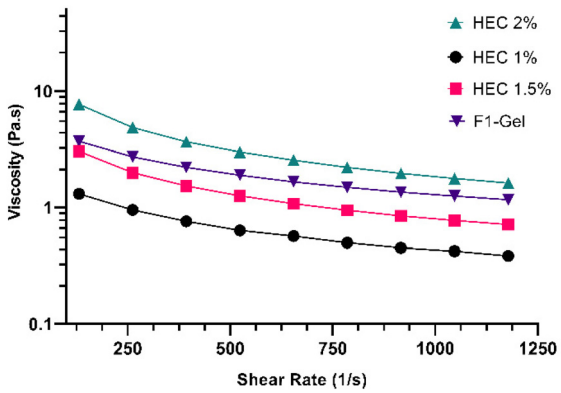

Fig. 5 Rheological characterization of blank hydroxyethyl cellulose gel and F1-gel.

3.5 Stability study of NAR-micelle formulation

The content of NAR in F1 micelles and its gel formulation was stable over the stability study period of 4 weeks at 25 °C as the NAR content retained in the formulations was >98% after storage (Fig. 6).

3.6 *In vitro* MIC testing

This study was designed to discover the potential of NAR to develop as an effective anti-acne drug. This research, to the best of our knowledge has been conducted, for the first time, revealing the ground-breaking potential of NAR against acne bacterial strains. The 31 isolates of pathogenic anaerobic bacterial strains of Gram-positive *C. acnes* and aerobic Gram-positive *S. aureus* and *S. epidermidis* tested in this study showed significant susceptibility to NAR and the NAR-micelle formulation evaluated using the agar dilution method (Tables 2 and 5). The antibacterial study results showed MIC_{50} of both NAR and NAR-micelle was 0.031 μg mL^{-1} against all 31 isolates of *C. acnes* (Table 4) whilst the MIC was found to be 0.5 μg mL^{-1} for NAR-micelle against Staphylococcus strains (Table 5). The MIC_{50} of NAR was revealed as 0.25 μg mL^{-1} which coincides with the MIC range of 0.125–1 μg mL^{-1} in the published reports against *S. aureus* strains.[58,59] These low MIC results indicate NAR's potential efficacy and remarkable activity against acne pathogens and hence potential as a topical therapeutic entity for resistant acne bacteria.

NAR, in common with other polyether ionophores, exhibits antibacterial activity through a novel mechanism that involves disrupting the EMF across the bacterial cell membranes by forming reversible dynamic complexes with cations that are soluble in lipids and by this means enable the transport of specific ions across biological membranes.[15,60] Due to its high lipophilicity, NAR is capable of penetrating the highly porous cell wall layer of Gram-positive bacteria, which is composed of peptidoglycan. This results in an introduction of an imbalanced ionic concentration gradient across the cell membrane,

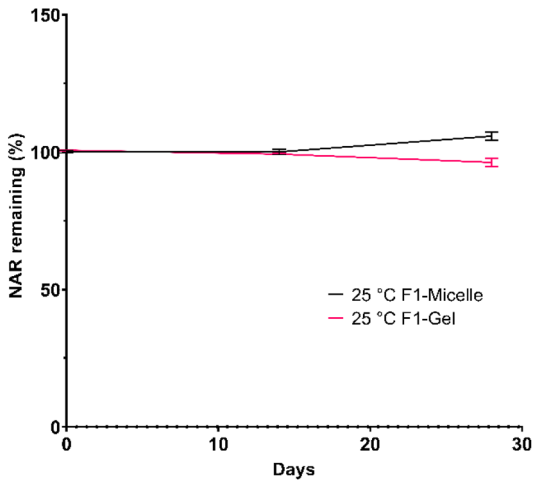

Fig. 6 Stability profile of F1-micele and F1-gel during storage for 4 weeks at 25 °C.

Table 2 MIC of NAR and NAR-micelle formulations against 31 isolates of *C. acnes* strains

Strain	MALDI IDs	NAR MIC (μg mL^{-1})	F1 MIC (μg mL^{-1})	F2 MIC (μg mL^{-1})	F3 MIC (μg mL^{-1})
00-1	*C. acnes*	≤0.008	≤0.008	≤0.008	≤0.008
00-2	*C. acnes*	0.062	>0.062	>0.062	>0.062
00-3	*C. acnes*	0.062	>0.062	>0.062	>0.062
00-4	*C. acnes*	≤0.008	≤0.008	≤0.008	≤0.008
00-5	*C. acnes*	≤0.008	≤0.008	≤0.008	≤0.008
00-6	*C. acnes*	≤0.008	0.031	0.031	0.062
00-7	*C. acnes*	0.062	0.062	>0.062	>0.062
00-8	*C. acnes*	0.031	0.062	0.062	0.062
00-9	*C. acnes*	0.062	0.062	>0.062	>0.062
0-10	*C. acnes*	0.062	0.062	>0.062	>0.062
0-12	*C. acnes*	≤0.008	≤0.008	≤0.008	≤0.008
0-13	*C. acnes*	>0.062	>0.062	>0.062	>0.062
0-14	*C. acnes*	0.062	0.031	>0.062	>0.062
0-15	*C. acnes*	≤0.008	≤0.008	≤0.008	≤0.008
0-16	*C. acnes*	0.016	≤0.008	>0.062	>0.062
0-18	*C. acnes*	≤0.008	≤0.008	≤0.008	≤0.008
0-19	*C. acnes*	≤0.008	≤0.008	≤0.008	≤0.008
0-20	*C. acnes*	>0.062	>0.062	>0.062	>0.062
0-21	*C. acnes*	≤0.008	≤0.008	0.016	≤0.008
0-22	*C. acnes*	≤0.008	≤0.008	≤0.008	≤0.008
0-23	*C. acnes*	0.062	0.062	0.062	0.062
0-24	*C. acnes*	≤0.008	≤0.008	≤0.008	≤0.008
0-25	*C. acnes*	>0.062	>0.062	>0.062	>0.062
0-26	*C. acnes*	0.062	>0.062	>0.062	>0.062
0-27	*C. acnes*	0.062	>0.062	>0.062	>0.062
0-28	*C. acnes*	≤0.008	≤0.008	≤0.008	≤0.008
0-29	*C. acnes*	0.062	>0.062	0.062	>0.062
0-30	*C. acnes*	0.062	0.062	0.031	0.062
0-31	*C. acnes*	0.062	>0.062	>0.062	>0.062
0-32	*C. acnes*	>0.062	>0.062	>0.062	>0.062
0-33	*C. acnes*	0.031	0.031	0.062	0.062

Table 3 The control antimicrobial QC range against *B. fragilis* ATCC 25285

QC strain	Control antimicrobials	Range (μg mL^{-1})	MIC obtained (μg mL^{-1})
Bacteroides fragilis ATCC 25285	Clindamycin	0.5–2	0.5

leading to a decrease in intracellular K^+ ion concentration and intracellular pH.[60] This creates a large gradient of K^+ that drives H^+ influx into the cells, which in turn stimulates increased ATPase activity to sustain an alkaline intracellular pH. In response to ionophore-mediated H^+ influx, bacterial H^+-ATPase activity may increase to efflux H^+, potentially leading to ATP pool depletion. This disruption of bacterial cell division may be a possible mechanism for cellular death.[61–63]

Table 5 MIC of NAR and NAR-micelle formulations against *S. aureus*, and *S. epidermidis* strains

Staphylococcus strains	NAR (μg mL^{-1})	F1 (μg mL^{-1})	F2 (μg mL^{-1})	F3 (μg mL^{-1})
S. aureus ATCC 29213	0.25	0.5	0.5	0.5
S. epidermidis ATCC 14990	0.25	0.5	0.5	0.5

3.7 Cell cytotoxicity assay (MTT assay)

Cytotoxicity provides important insights for cell viability, therefore, in this study we considered MTT assay to investigate the effect of different concentrations of NAR and F1-micelle formulations on the HFFs (Fig. 7B) and HaCaT cell lines (Fig. 7A). The skin is the largest organ, additionally, it is also an important target site for application of topical formulations for the treatment of superficial skin conditions.[64] In this study, the treated cells with NAR showed a decrease in percentage cell viability after 24 h incubation between concentrations 0.06–4 μg mL^{-1}. The percentage cell viability of cells treated with NAR-micelle formulation was, however, comparatively higher at the same concentrations suggesting that NAR-micelle formulation has less toxicity compared to NAR at higher concentrations (Fig. 7). The NAR-micelle formulation, therefore, may enable potential topical therapeutic application against resistant acne disease due to its low toxicity at concentrations exhibiting potential activity against Gram-positive and Gram-negative bacteria.

3.8 *Ex vivo* NAR permeation and deposition studies

Skin permeation and deposition of NAR from the F1-micelle solution and the F1-gel were evaluated and compared to the NAR-water solution after 24 h application to full-thickness pig skin under infinite dose conditions (1 g cm^{-2} – *i.e.*, 2 mg NAR per cm^2 for the F1-micelle (0.2%) and F1-gel (0.2%), 0.01 mg NAR per cm^2 for the NAR-water). The amount of NAR deposited from the skin surface across the stratum corneum, epidermis, dermis, and receptor chamber were determined as shown in Fig. 8. The amount of NAR recovered from the skin surface using F1-gel (7068.79 ± 588.31 ng cm^{-2}) was statistically significant and less than that observed with F1-micelle (27 063.47 ± 805.98 ng cm^{-2}), whereas the amount of NAR deposited in the epidermis was similar between micelle solution (19 347 ± 1912.98 ng cm^{-2}) and the F1-gel (18 763.54 ± 580.77 ng cm^{-2}), however, significantly more NAR was found in the stratum corneum using F1-gel formulation (40 601.14 ± 3736.09 ng cm^{-2}) compared with the micelle solution (19 835.60 ± 6237.89 ng cm^{-2}) ($p < 0.0001$), and significantly

Table 4 MIC_{50}, MIC_{90}, and MIC range of NAR and NAR-micelle formulations against 31 isolates of *C. acnes* strains

C. acnes (μg mL^{-1})	NAR	F1	F2	F3
MIC_{50}	0.031	0.031	0.062	0.062
MIC_{90}	>0.062	>0.062	>0.062	>0.062
MIC range	≤0.008–0.062	≤0.008–0.062	≤0.008–0.062	≤0.008–0.062

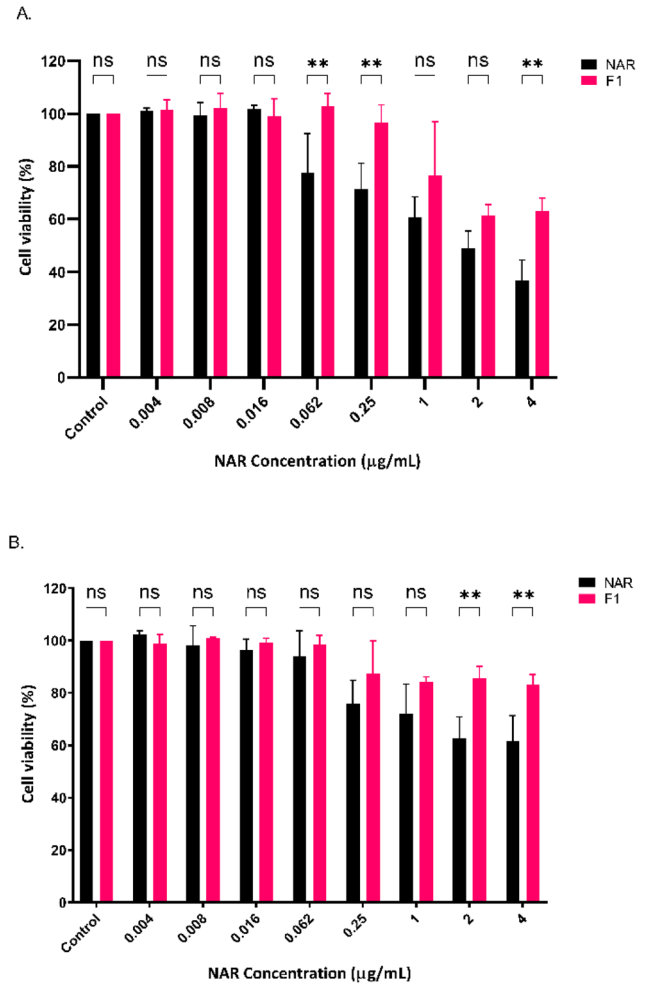

Fig. 7 MTT assay of different concentrations of NAR and F1-micelle formulation on (A) HaCaT and (B) HFF-1 cell line. 2-way ANOVA and Sidak's multiple comparison tests were employed to determine statistical differences. **, $p < 0.01$.

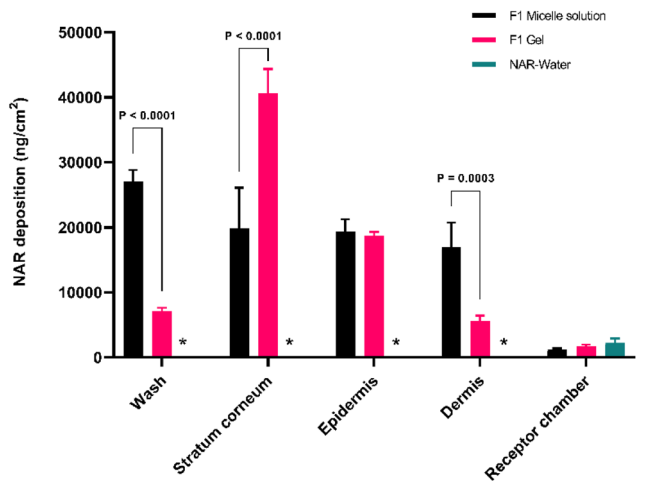

Fig. 8 *Ex vivo* NAR skin deposition and permeation after 24 hours from the F1 micelle solution and F1 gel using full-thickness pig ear skin. The results are displayed as the mean ± SD ($n = 3$); the p-value is displayed when there is a significant difference. * indicates NAR in water solution not detected.

less in the dermis layer(16 906.84 ± 3831.61 ng cm^{-2} for F1-micelle, and 5638.76 ± 795.86 ng cm^{-2} for F1-gel) ($p = 0.0003$).

Based upon the outcomes of this study with the F1-micelle solution and the gel formulation compared to the NAR-water solution, it was concluded that SOL present in the micelles yielded bioadhesive characteristics, prolonging the residence time of NAR on the skin, thereby allowing greater contact with the stratum corneum.[36] Furthermore, the difference in the deposition profile of NAR in micelle solution and gel formulation could be due to the additional bioadhesion provided by the HEC, the polymeric component, further increasing the contact time between the skin and the gel formulation.[65] Interestingly, no NAR was detected in any skin layer using the NAR-water solution, which demonstrated the superiority of the developed formulation as it ensured localized delivery of NAR to the stratum corneum and epidermis, the desired site for acne treatment.[53] Furthermore, since NAR is insoluble in the aqueous phase, the incorporation of NAR into micelles will generate a saturated or supersaturated system allowing a high concentration gradient for its release and partitioning into the lipophilic skin layers, stratum corneum and epidermis, depending on the NAR affinity with the surrounding tissue environment. Additionally, the potential role of nanometer size of micelles also plays a significant role in the release and selective delivery into the lipophilic skin because of easier penetration into the hair follicular structures (site of acne treatment).[66]

Controlling the permeation of NAR across the skin was also considered to prevent unwanted systemic toxicity and therefore NAR was applied, under infinite dose conditions, in much greater quantity than expected in the clinical setting, where much lower quantities are administered, to study the extent of permeation across the skin. The NAR recovered after 24 h application of the F1-micelle solution, F1-gel formulation, and NAR-water solution was found to be 1247.54 ± 148.20, 1723.98 ± 268.34, and 2262.79 ± 654.71 ng cm^{-2} respectively (equivalent to the concentration of 0.80, 1.10, and 1.45 μg mL^{-1} respectively). The results from the cell safety studies (as mentioned under cell viability assay) conducted at these concentrations for the micelle formulation indicate its safe use for topical application, however, NAR-water solution demonstrated lower cell viability (<80%) indicating a potential risk for skin application. Limited transdermal penetration under infinite dose conditions suggests the unlikelihood of NAR causing systemic toxicity in the *in vivo* models and clinical settings (where even lower amounts are applied), however, determining the potential side effect profile of NAR requires formulating preclinical and clinical investigations to establish its potential efficacy. Therefore, optimizing rational topical dosage forms can assist minimize the risk of unwanted side effects.

4 Conclusions

Acne vulgaris, associated with infection by *C. acnes* is a prevalent skin condition severely affecting individuals globally. The

marketed treatment formulations are mostly associated with the potential risk of adverse effects and the long-term use of marketed antibiotic formulations, has led to the emergence of antimicrobial resistance, and therefore developing a novel antibiotic that is safe for use is an unmet clinical need. Here, the novel antibacterial activity of NAR was utilized against human isolates of *C acnes*. A stable NAR-nano micelle formulation was developed and characterized using SOL to translate NAR into an effective therapeutic agent for topical applications. The micelle formulation was able to effectively deliver NAR in the targeted site *i.e.*, stratum corneum and epidermis, as opposed to NAR in water at safer therapeutic concentrations. Thus, the presented research demonstrates that NAR has the potential to be developed into an effective anti-acne therapeutic agent and the nano micelles can ensure safe targeted topical delivery of NAR. Additionally, the SOL-based SNMSDs have the potential to improve the aqueous solubility of poorly water-soluble compounds.

Conflicts of interest

There are no conflicts to declare.

Acknowledgements

We would like to thank Future Industries Institute, University of South Australia, for DSC, and SEM analysis. We would also like to acknowledge Adelaide Microscopy, The University of Adelaide, for providing the facility for TEM analysis. We would like to particularly acknowledge Dr Jenny Robson and the staff of Sullivan Nicolaides Pathology, Queensland for the provision of clinical isolates of *Cutibacterium acnes*. FA would also like to thank Turki Alsaeed, Franklin Afinjuomo, Thabata Muta, Aurelia Elz, and Muhammad Awad for their support. Finally, we would like to express our gratitude to the reviewers for their discerning and astute remarks.

References

1 S. A. Alshammari, Y. Alamri, A. M. Alanazi, S. A. Almuhanna, L. Pinjabi and N. A. Alsnaidi, *Saudi Pharm. J.*, 2020, **28**, 374–379.
2 L. Ördögh, *Acta Biol. Szeged.*, 2010, **54**, 45–49.
3 M. A. Rocha and E. Bagatin, *Clin., Cosmet. Invest. Dermatol.*, 2018, **11**, 59–69.
4 D. Well, *J. Dermatol. Nurses' Assoc.*, 2014, **6**, 302–309.
5 A. Tan, B. J. Schlosser and A. Paller, *Int. J. Women's Dermatol.*, 2018, **4**, 56–71.
6 P. Wolkenstein, A. Machovcová, J. C. Szepietowski, D. Tennstedt, S. Veraldi and A. Delarue, *J. Eur. Acad. Dermatol. Venereol.*, 2018, **32**, 298–306.
7 X. Huang, J. Zhang, J. Li, S. Zhao, Y. Xiao, Y. Huang, D. Jing, L. Chen, X. Zhang, J. Su, Y. Kuang, W. Zhu, M. Chen, X. Chen and M. Shen, *J. Pediatr.*, 2019, **204**, 256–262.
8 C. N. Jayasena and S. Franks, *Nat. Rev. Endocrinol.*, 2014, **10**, 624–636.
9 A. Bianconi-Moore, *Nurs. Stand.*, 2012, **26**, 43–49.
10 G. Josse, C. Mias, J. Le Digabel, J. Filiol, C. Ipinazar, A. Villaret, C. Gomiero, M. Bevilacqua, D. Redoules, T. Nocera, J. H. Saurat and E. Gontier, *Exp. Dermatol.*, 2020, **29**, 168–176.
11 A. L. Zaenglein, A. L. Pathy, B. J. Schlosser, A. Alikhan, H. E. Baldwin, D. S. Berson, W. P. Bowe, E. M. Graber, J. C. Harper, S. Kang, J. E. Keri, J. J. Leyden, R. V. Reynolds, N. B. Silverberg, L. F. Stein, M. M. Tollesfon, J. S. Weiss, N. C. Dolan, A. A. Sagan, M. Stern and R. Bhushan, *J. Am. Acad. Dermatol.*, 2016, **74**, 945–973.
12 J. S. Barbieri, W. D. James and D. J. Margolis, *J. Am. Acad. Dermatol.*, 2017, **77**, 456–463.
13 J. S. Barbieri, K. Bhate, K. P. Hartnett, K. E. Fleming-Dutra and D. J. Margolis, *JAMA Dermatol.*, 2019, **155**, 290–297.
14 J. Paik, *Am. J. Clin. Dermatol.*, 2020, **21**, 449–456.
15 D. A. Kevin II, D. A. Meujo and M. T. Hamann, *Expert Opin. Drug Discovery*, 2009, **4**, 109–146.
16 D. H. Berg and R. L. Hamill, *J. Antibiot.*, 1978, **31**, 1–6.
17 J. S. Y. Low, K. X. Wu, K. C. Chen, M. Ng and J. Chu, *Antiviral Ther.*, 2011, **16**, 1203.
18 B. S. Makhmalzade and F. Chavoshy, *J. Adv. Pharm. Technol. Res.*, 2018, **9**, 2.
19 A. A. Date, B. Naik and M. S. Nagarsenker, *Skin Pharmacol. Physiol.*, 2006, **19**, 2–16.
20 Y. Bachhav, K. Mondon, Y. Kalia, R. Gurny and M. Möller, *J. Controlled Release*, 2011, **153**, 126–132.
21 M. Lapteva, K. Mondon, M. Möller, R. Gurny and Y. N. Kalia, *Mol. Pharm.*, 2014, **11**, 2989–3001.
22 M. Lapteva, V. Santer, K. Mondon, I. Patmanidis, G. Chiriano, L. Scapozza, R. Gurny, M. Möller and Y. N. Kalia, *J. Controlled Release*, 2014, **196**, 9–18.
23 M. Lapteva, M. Möller, R. Gurny and Y. N. Kalia, *Nanoscale*, 2015, **7**, 18651–18662.
24 D. Gabriel, T. Mugnier, H. Courthion, K. Kranidioti, N. Karagianni, M. C. Denis, M. Lapteva, Y. Kalia, M. Möller and R. Gurny, *J. Controlled Release*, 2016, **242**, 16–24.
25 E. Kahraman and S. Güngör, *Colloids Surf., B*, 2016, **146**, 692–699.
26 S. G. Kandekar, S. del Río-Sancho, M. Lapteva and Y. N. Kalia, *Nanoscale*, 2018, **10**, 1099–1110.
27 R. Pignatello, R. Corsaro, A. Bonaccorso, E. Zingale, C. Carbone and T. Musumeci, *Drug Delivery Transl. Res.*, 2022, **12**, 1991–2006.
28 A. Parikh, K. Kathawala, Y. Song, X.-F. Zhou and S. Garg, *Drug Delivery Transl. Res.*, 2018, **8**, 1389–1405.
29 M. Linn, E.-M. Collnot, D. Djuric, K. Hempel, E. Fabian, K. Kolter and C.-M. Lehr, *Eur. J. Pharm. Sci.*, 2012, **45**, 336–343.
30 L. Dian, E. Yu, X. Chen, X. Wen, Z. Zhang, L. Qin, Q. Wang, G. Li and C. Wu, *Nanoscale Res. Lett.*, 2014, **9**, 1–11.

31 I. S. Jin, M. J. Jo, C.-W. Park, Y. B. Chung, J.-S. Kim and D. H. Shin, *Pharmaceutics*, 2020, **12**, 1000.
32 R. N. Shamma and M. Basha, *Powder Technol.*, 2013, **237**, 406–414.
33 J. Liu, M. Zou, H. Piao, Y. Liu, B. Tang, Y. Gao, N. Ma and G. Cheng, *Molecules*, 2015, **20**, 11345–11356.
34 A. Di Michele, G. Fredi, C. Pagano, A. Dorigato, P. Calarco, S. Primavilla, F. Marmottini, M. Ricci, A. Pegoretti and L. Perioli, *Appl. Clay Sci.*, 2022, **216**, 106377.
35 R. Takayama, M. Ishizawa, M. Yamada, Y. Inoue and I. Kanamoto, *ChemEngineering*, 2021, **5**, 44.
36 M. Nasr, H. Karandikar, R. T. Abdel-Aziz, N. Moftah and A. Paradkar, *Expert Opin. Drug Delivery*, 2018, **15**, 1165–1173.
37 F. Abid, S. H. Youssef, Y. Song, A. Parikh, D. Trott, S. W. Page and S. Garg, *Microchem. J.*, 2021, 107149.
38 CLSI, *Clinical and Laboratory Standards Institute*, 2018, **9**, 15–20.
39 C. Herkenne, A. Naik, Y. N. Kalia, J. Hadgraft and R. H. Guy, *Pharm. Res.*, 2006, **23**, 1850–1856.
40 S. Kim, S. Abdella, F. Abid, F. Afinjuomo, S. H. Youssef, A. Holmes, Y. Song, S. Vaidya and S. Garg, *Int. J. Nanomed.*, 2023, 1007–1029.
41 J. Lademann, U. Jacobi, C. Surber, H.-J. Weigmann and J. Fluhr, *Eur. J. Pharm. Biopharm.*, 2009, **72**, 317–323.
42 F. Abid, S. H. Youssef, Y. Song, A. Parikh, D. Trott, S. W. Page and S. Garg, *Microchem. J.*, 2022, **175**, 107149.
43 H. Danafar, S. Davaran, K. Rostamizadeh, H. Valizadeh and M. Hamidi, *Adv. Pharm. Bull.*, 2014, **4**, 501.
44 G. Gaucher, R. H. Marchessault and J.-C. Leroux, *J. Controlled Release*, 2010, **143**, 2–12.
45 H. A. A. Hussein and N. K. Maraie, *Mater. Today: Proc.*, 2022, **61**, 672–680.
46 P. Jadhav, C. Bothiraja and A. Pawar, *J. Pharm. Innovation*, 2018, **13**, 213–225.
47 H. K. Manjili, H. Malvandi, M. S. Mousavi, E. Attari and H. Danafar, *Artif. Cells, Nanomed., Biotechnol.*, 2018, **46**, 926–936.
48 H. Zhang, L. Zhao, L. Chu, X. Han and G. Zhai, *J. Colloid Interface Sci.*, 2014, **434**, 40–47.
49 J. F. Alopaeus, E. Hagesæther and I. Tho, *Pharmaceuticals*, 2019, **12**, 15.
50 A. Parikh, K. Kathawala, Y. Song, X.-F. Zhou and S. Garg, *Drug Delivery Transl. Res.*, 2018, **8**, 1389–1405.
51 H. Wu, K. Wang, H. Wang, F. Chen, W. Huang, Y. Chen, J. Chen, J. Tao, X. Wen and S. Xiong, *Colloids Surf., B*, 2017, **149**, 97–104.
52 N.-Q. Shi, H.-W. Lai, Y. Zhang, B. Feng, X. Xiao, H.-M. Zhang, Z.-Q. Li and X.-R. Qi, *Pharm. Dev. Technol.*, 2018, **23**, 573–586.
53 J. Lademann, F. Knorr, H. Richter, S. Jung, M. Meinke, E. Rühl, U. Alexiev, M. Calderón and A. Patzelt, *J. Innovative Opt. Health Sci.*, 2015, **8**, 1530004.
54 J. Lademann, H. Richter, S. Schanzer, F. Knorr, M. Meinke, W. Sterry and A. Patzelt, *Eur. J. Pharm. Biopharm.*, 2011, **77**, 465–468.
55 A. Patzelt and J. Lademann, *Expert Opin. Drug Delivery*, 2013, **10**, 787–797.
56 R. Su, W. Fan, Q. Yu, X. Dong, J. Qi, Q. Zhu, W. Zhao, W. Wu, Z. Chen and Y. Li, *Oncotarget*, 2017, **8**, 38214.
57 M. Lukić, I. Pantelić and S. D. Savić, *Cosmetics*, 2021, **8**, 69.
58 W. Y. Chan, E. E. Hickey, M. Khazandi, S. W. Page, D. J. Trott and P. B. Hill, *Vet. Dermatol.*, 2018, **29**, 149–e57.
59 E. E. Hickey, H. S. Wong, M. Khazandi, A. D. Ogunniyi, K. R. Petrovski, S. Garg, S. W. Page, R. O'Handley and D. J. Trott, *J. Vet. Pharmacol. Ther.*, 2018, **41**, 746–754.
60 J. B. Russell and H. Strobel, *Appl. Environ. Microbiol.*, 1989, **55**, 1–6.
61 P. Butaye, L. A. Devriese and F. Haesebrouck, *Clin. Microbiol. Rev.*, 2003, **16**, 175–188.
62 T. Callaway, T. Edrington, J. Rychlik, K. Genovese, T. Poole, Y. S. Jung, K. Bischoff, R. Anderson and D. J. Nisbet, *Curr. Issues Intest. Microbiol.*, 2003, **4**, 43–51.
63 B. C. Pressman, *Annu. Rev. Biochem.*, 1976, **45**, 501–530.
64 A. Nair, S. Jacob, B. Al-Dhubiab, M. Attimarad and S. Harsha, *Braz. J. Pharm. Sci.*, 2013, **49**, 423–434.
65 D. S. Jones, A. D. Woolfson and A. F. Brown, *Int. J. Pharm.*, 1997, **151**, 223–233.
66 D. Papakostas, F. Rancan, W. Sterry, U. Blume-Peytavi and A. Vogt, *Arch. Dermatol. Res.*, 2011, **303**, 533–550.